



Optimization of p-type HPGe detector model using Monte Carlo simulation

Le Thi Ngoc Trang^{1,3} · Huynh Dinh Chuong^{1,3} · Tran Thien Thanh^{2,3}

Received: 11 August 2020 / Accepted: 18 October 2020 / Published online: 30 October 2020
© Akadémiai Kiadó, Budapest, Hungary 2020

Abstract

In this study, the optimization of the p-type HPGe detector model has been performed to improve the accuracy of Monte Carlo simulation in calculating full energy peak efficiency. The optimized detector model was validated by comparison of simulated efficiencies with experimental efficiencies for measurement configurations of point-like sources at various distances from the detector surface and cylindrical sources on the detector surface. The obtained results showed an excellent agreement between the simulated and experimental efficiencies with relative deviations of less than 4% in the energy range from 53 to 1847 keV.

Keywords Dead layer · Full energy peak efficiency · HPGe detector · Monte Carlo simulation · MCNP

Introduction

Low background gamma-ray spectrometers with high-purity germanium (HPGe) detectors are widely applied for identifying and quantifying gamma-emitting radionuclides present in the environmental samples and radioactive waste. For these applications, accurate knowledge of full energy peak (FEP) efficiency appropriate to the specific measurement conditions of each analyzed sample is required to obtain high-quality results. In recent years, Monte Carlo simulation is often used to determine the FEP efficiency of detectors. In such cases, the accuracy of the simulated efficiency must be evaluated before it is used for the determination of the activity of radionuclides in the analyzed samples. The problem is how to achieve the well-simulated efficiencies that match the experimental efficiencies for the interested measurement configurations. Basically, the quality of simulated results depends on the accuracy of codes used to simulate the physical processes of interest and on the quality of input

data. Nowadays, several general-purpose Monte Carlo codes such as GEANT4 [1], MCNP [2], PENELOPE [3] have been developed to simulate the transport of ionizing radiation, to solve the problems related to nuclear physics. With the experience from our previous studies [4–9], these codes are reliable enough to be used for the determination of the detection efficiency of gamma-ray spectrometers. Besides, the input data must contain information about geometry, materials, and physical processes involved in radiation transport, to construct the simulation model to be as close to the experimental conditions as possible. For this task, detailed knowledge about the detector characteristics, lead shielding, radioactive sources are required.

Usually, most of the information required for the input data can be found on the datasheet provided by the manufacturers. However, many previous studies have reported that the experimental FEP efficiencies are significantly different from the simulated FEP efficiencies based on the HPGe detector model constructed by the manufacturer's specifications [6, 10–15]. These studies have also shown that the discrepancy is mainly related to the deviation between the nominal and real values of the dead-layer thickness. In the coaxial p-type HPGe detectors, the important dead-layer is an n_+ contact made with diffused lithium atoms on the top and lateral surfaces of the germanium crystal. This layer behaves as an inactive region with low or zero charge collection efficiency, so it can not contribute to the counts in the full energy peak region. Besides, it plays the role of an

✉ Huynh Dinh Chuong
hdchuong@hcmus.edu.vn

¹ Nuclear Technique Laboratory, University of Science, 227 Nguyen Van Cu Street, District 5, Ho Chi Minh City, Vietnam

² Faculty of Physics and Engineering Physics, University of Science, Ho Chi Minh City, Vietnam

³ Vietnam National University, Ho Chi Minh City, Vietnam

absorber layer surrounding the active volume of the germanium crystal, and hence affecting the FEP efficiency of the detector, especially in the low energy region (below 100 keV). The increase of the dead-layer thickness over periods of the life-time of the HPGe detector has also been observed due to the continuous diffusion of the lithium atoms into the germanium crystal [16]. Besides, there may also be the deviations in the other detector parameters such as the diameter and length of the crystal, the diameter and depth of hole in the crystal, round edge of the crystal, the distance from crystal to front endcap, etc. The influence of these parameters on the FEP efficiency has been studied by some authors [17, 18]. The results showed that slight variations of the parameters can cause significant differences in FEP efficiency. Therefore, optimization of the detector model is necessary to improve the accuracy of the simulated FEP efficiency, especially in the case of old detectors.

In general, two approaches can be classified for the optimization of an HPGe detector model in Monte Carlo simulation. The first approach involves accurately determining the values of the geometric parameters for the surveyed detector using various techniques. For example, the inner structure and physical dimensions of the detector can be determined by gamma/X-ray radiography [6, 10, 11, 19]; the dimensions of the active volume of the germanium crystal and the non-uniformity of the dead-layer can be determined by a combination of gamma scanning and Monte Carlo simulation [20–23]. The detector model constructed by these defined values is close to the real detector, therefore it is reliable enough to be used in Monte Carlo simulations for all measurement configurations. However, this approach is difficult to implement for many laboratories, because the conditions for applying the X-ray radiography and gamma scanning techniques are not always convenient or available. The second approach involves experimental calibration of the FEP efficiency for simple measurement configurations and trying to adjust the dead-layer thickness and various parameters in the detector model to reach a good agreement between simulated and experimental results. Many studies have been performed for the optimization of the p-type HPGe detector model based on the second approach [12–15, 24–26]. In most of these studies, an agreement between simulated and experimental efficiencies within 5% was achieved at energies above 100 keV. The advantages of the second approach are simplicity and quick to implement in laboratories. However, the optimized detector model obtained from this approach is not guaranteed to be close to the real detector. Since the simulated FEP efficiencies depend on many detector parameters, there may be various detector models that satisfy the agreement between simulated and experimental efficiencies for surveyed measurement configurations. Therefore, it would not be reliable enough to be used in Monte Carlo simulations for the calculation of FEP efficiency with different

measurement configurations. In our opinion, the validity of the optimized detector model should be verified for specific measurement configurations that are similar to those of the analyzed samples.

The present study proposed a simple procedure based on the second approach for optimizing the model of coaxial p-type HPGe detector in Monte Carlo simulation. The procedure only requires experimental calibration of the FEP efficiencies in the energy range of 53–1770 keV for the measurement configurations of the point-like source at distances of 54 mm and 254 mm from the detector surface. MCNP code version 6 (MCNP6) [27] was used for Monte Carlo simulation of photon transport. First, an initial detector model was constructed based on the manufacturer's specifications. Then, the values of detector parameters including the thickness of the lateral dead-layer, the thickness of the top dead-layer, and the distance from crystal to front endcap were adjusted step-by-step to achieve the optimized detector model. In each step, specific experimental FEP efficiencies (corresponding to different photon energies and measurement configurations) were selected to compare with simulated FEP efficiencies. The values of these experimental FEP efficiencies are considered to depend only on the interested parameter. In other words, the influence of the remaining parameters on these FEP efficiencies is insignificant. The use of the optimized detector model in Monte Carlo simulations enables to guarantee minimum deviations between the simulated and experimental efficiencies in the energy range of 53–1770 keV for measurement configurations of the point-like source at different distances from the detector surface. Finally, the validity of the optimized detector model was checked for measurement configurations of cylindrical samples on the detector surface. The goodness of simulated results to experimental data is the basis for evaluating the reliability of the proposed procedure.

Experimental setup

A low background gamma-ray spectrometer with a coaxial p-type HPGe detector (model GC3520 of Mirion Inc.) was used in this study. The HPGe detector has a typical relative efficiency of 35% and an energy resolution of 2.0 keV for the ^{60}Co gamma-ray at 1332 keV. This detector with a pre-amplifier was connected to LYNX, which includes high-voltage power supply, amplifier, and multi-channel analyzer (MCA) based on advanced digital signal processing techniques [28]. The acquisitions of gamma spectra were driven by GENIE-2 k software version 3.3. All spectra were recorded with the mode of 32,768 channels and the energy width per channel of 89.92 eV to detect photons in the energy range up to 2946 keV. The HPGe detector was installed inside a lead shielding (model 747 of Mirion Inc.)

for achieving a low background needed in environmental applications. The structure of the lead shielding consists from outside of 9.5 mm stainless steel, 100 mm graded lead, liners of 1 mm tin and 1.6 mm copper to reduce the contribution of the lead X-rays in the spectra [29].

The standard radioactive sources (type D configuration of Eckert & Ziegler Group), including ^{22}Na , ^{54}Mn , ^{57}Co , ^{60}Co , ^{65}Zn , ^{109}Cd , ^{133}Ba , ^{137}Cs , ^{154}Eu , ^{207}Bi , and ^{241}Am with the activities approximately 37,000 Bq were used to provide gamma-rays in the energy range of 53–1770 keV. The sources are disk-shaped made of high strength plastic with a diameter of 25.4 mm and a thickness of 6.35 mm; the active diameter of the source is 5 mm, and the window thickness is 2.77 mm [30]. These sources can be considered point-like sources because of their small dimensions. The point-like sources were measured at different positions on the symmetry axis of the detector with distances of 54, 154, and 254 mm from the detector surface. For such measurements, the sources were placed on a support made of PMMA (Polymethyl methacrylate) plastic.

Besides, two cylindrical reference samples (denoted by S1 and S2) were measured on the detector surface. The S1 sample was made by diluting 0.25 ml of the standard radioactive solution (series 7503 of Eckert and Ziegler [31]) in 500 ml of 2M HCl acid solution. This diluted solution was contained inside a cylindrical container with an inner diameter of 66 mm, the wall thickness of 0.5 mm, and bottom thickness of 3 mm; the height and density of the solution filled in the container are 143.5 mm and 1.03 g cm^{-3} , respectively. This sample includes radionuclides such as ^{57}Co , ^{60}Co , ^{85}Sr , ^{88}Y , ^{109}Cd , ^{113}Sn , $^{123\text{m}}\text{Te}$, ^{137}Cs , ^{210}Pb , and ^{241}Am that provide gamma-rays in the energy range of 47–1836 keV. The S2 sample was prepared by storing the IAEA-RGU-1 reference material (supplied by the International Atomic Energy Agency) inside a cylindrical container with the inner diameter of 73 mm, the wall and bottom thickness of 2 mm; the height and density of the material filled in the container are 20.125 mm and 1.5451 g cm^{-3} , respectively. The S2 sample was measured after a waiting time of 30 days for achieving the secular equilibrium of the decay chain ^{238}U . This sample emits gamma-rays with energies in the range of 47–2448 keV. The elemental composition of the IAEA-RGU-1 material was also determined by WDXRF spectrometer (S8 TIGER Series of Bruker) with the following result: O—53.1519%, Si—46.4653%, Al—0.1279%, Ca—0.1051%, Fe—0.0514%, K—0.0349%, U—0.0278%, Ti—0.0126%, S—0.0084%, Pb—0.0078%, Cu—0.0039%, Zr—0.0030%. These data were used to construct the simulation models to ensure the similarity between the simulation and the experiment.

The acquisition time for each spectrum was adjusted to keep the statistical uncertainty of the interested peak area below 1%. The dead-time for all measurements is less than

4%. However, the analyzer automatically corrects dead-time losses because the MCA works in the live-time mode.

For the data analysis, the background spectrum was subtracted from the spectra obtained with the radioactive sources. Then, these spectra were processed by the COLEGRAM software that uses the least-squares method to fit mathematical functions to experimental data [32]. The interested peaks were fitted by the Gaussian function to obtain the net area, while the background was fitted by the one-step function or the polynomial function in COLEGRAM. The choice of an appropriate function for the fitting background depends on the experience of the analyst with the data region of interest. The experimental FEP efficiency and its relative uncertainty were determined by the following equations:

$$\varepsilon_{\text{Exp.}}(E) = \frac{N(E)}{A \times I_{\gamma}(E) \times t} \times C_{\text{Coin.}} \times C_{\text{decay}} \quad (1)$$

$$u_{\varepsilon_{\text{Exp.}}} = \sqrt{(u_N)^2 + (u_A)^2 + (u_{I_{\gamma}})^2 + (u_{C_{\text{decay}}})^2} \quad (2)$$

where N is the net area of an interested peak; A is the activity of source (Bq); I_{γ} is the photon emission probability; t is the live acquisition time (s); C_{decay} is the decay correction factor for the decline of the activity over time; $C_{\text{Coin.}}$ is the coincidence summing correction factor (CSF) for the complex decay-scheme radionuclides. Besides, u_N , u_A , $u_{I_{\gamma}}$ and $u_{C_{\text{decay}}}$ are the relative uncertainty of the net area, the activity, the photon emission probability, and the decay correction factor, respectively. The values of photon energy, photon emission probability, half-life, and their uncertainties for radionuclides were given from the recommended data of Laboratoire National Henri Becquerel [33].

Monte Carlo simulations

In this study, MCNP6 code was used to calculate the FEP efficiency of the HPGe detector. MCNP-CP code, which is an extended version of MCNP4C code for Monte Carlo simulations with a source of correlated nuclear particles [34], was used to calculate the CSF for the complex decay scheme radionuclides. This code allows us to perform a statistical simulation of processes accompanying radioactive decay of a specified radionuclide, yielding characteristics of emitted correlated characteristics of emitted particles, which are then tracked within the same history. The method for the calculation of the CSF using MCNP-CP code was described in some previous studies [35, 36]. To use these codes, the information about the HPGe detector, radioactive source, lead shielding, and support corresponding to the surveyed measurement configurations (as described in the [experimental setup](#) section) was declared in the input files.

The cross-sections of the simulated geometry for the entire measurement configuration with the point-like source at a distance of 254 mm and HPGe detector are shown in Fig. 1. The specifications used in the initial detector model and the optimized detector model are given in Table 1.

In input files, the radioactive sources were setup to emit only photons and the transport of primary and secondary

photons was simulated. The databases of photon interaction and atomic relaxation (from ENDF/B-VI.8 release) are included in the new electron-photon-relaxation data library (eprdata12). The cut-off energy for the photons was setup at 1 keV. The F8 tally, available in MCNP6 and MCNP-CP codes, was used to obtain the pulse height spectrum. This is the probability spectrum which gives the distribution of

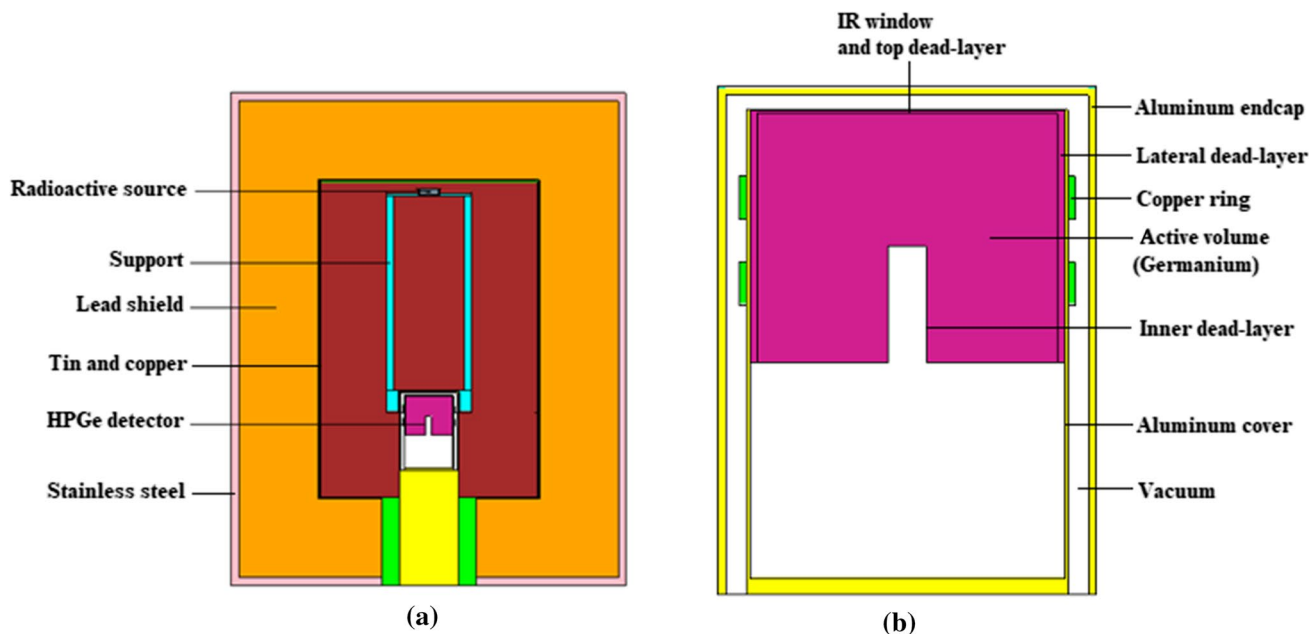


Fig. 1 Cross-section of the simulation model for **a** entire measurement configuration and **b** HPGe detector in MCNP6 code

Table 1 Specifications of the HPGe detector used in Monte Carlo simulations

Description	Value from initial model	Value from optimal model
Diameter of Ge crystal	62.2 mm	62.2 mm
Length of Ge crystal	50.1 mm	50.1 mm
Distance from Ge crystal to front endcap	5.0 mm	5.0 mm
Hole diameter in Ge crystal	7.5 mm	7.5 mm
Hole depth in Ge crystal	23.0 mm	23.0 mm
Thickness of top dead-layer	0.46 mm	0.52 mm
Thickness of lateral dead-layer	0.46 mm	1.31 mm
Thickness of inner dead-layer	0.0003 mm	0.0003 mm
Thickness of mylar in IR window	0.00847 mm	0.00847 mm
Thickness of kapton in IR window	0.1016 mm	0.1016 mm
Thickness of Al endcap	1.5 mm	1.5 mm
Diameter of Al endcap	75 mm	75 mm
Density of Ge crystal	5.35 g cm ⁻³	5.35 g cm ⁻³
Density of Ge dead-layer	5.35 g cm ⁻³	5.35 g cm ⁻³
Density of Mylar	1.38 g cm ⁻³	1.38 g cm ⁻³
Density of Kapton	1.42 g cm ⁻³	1.42 g cm ⁻³
Density of Al endcap	2.699 g cm ⁻³	2.699 g cm ⁻³

deposited energy per photon inside the active volume of the HPGe detector at different energy bins. The energy bins in the simulated spectra were setup based on the energy calibration obtained from the experiments. The mono-energetic sources were used for the calculation of the FEP efficiency. The photons considered for the evaluation of the FEP efficiency are those that undergo a complete absorption of their energy in the detector. The number of photons emitted from the radioactive source was adjusted for each measurement configuration to ensure the relative uncertainty of the simulated FEP efficiency less than 0.5%.

Procedure description

In the present study, a procedure was proposed for optimizing the model of p-type HPGe detector. First, an initial detector model was constructed based on the manufacturer's specifications (as given in Table 1). Then, three parameters of this detector model including the thickness of the lateral dead-layer, the thickness of the top dead-layer, and the distance from crystal to front endcap were adjusted step-by-step to achieve the optimized detector model. It is worth noting that the lateral dead-layer and the top dead-layer were adjusted separately and different thicknesses of these layers were expected. The experimental FEP efficiencies in the energy range of 53–1770 keV for the measurement configurations of a point-like source at two distances of 54 mm and 254 mm from the detector surface were used to optimize the detector model. For the measurement configuration of the point-like source at a distance of 54 mm, only mono-energetic sources including ^{54}Mn , ^{65}Zn , ^{109}Cd , ^{137}Cs , and ^{241}Am were considered, to exclude the coincidence summing effects. Whole experimental FEP efficiencies for measurement configuration of the point-like source at a distance of 254 mm were used because the coincidence summing effects can be considered as insignificant at this distance [19]. Therefore, the optimization of the detector model is

not affected by the coincidence summing effects. The steps for this procedure were summarized in Fig. 2.

For the adjustment of each parameter, Monte Carlo simulations were performed with the variations in the value of interested parameter to calculate the FEP efficiencies. The simulated FEP efficiencies versus the values of interested parameter were fitted by the least-squares method to determine the desired equations corresponding to different photon energies. The interpolated values of the interested parameter were determined by substituting the experimental FEP efficiencies into the obtained equations, respectively. The average of these interpolated values, which is considered as the optimized value, was used to adjust the interested parameter in the detector model. It should be noted that the order of the steps for adjusting the parameters is essential. Besides, in each step, the used FEP efficiencies must be suitable for the adjustment of interested parameter.

The first adjustment was made for the thickness of the lateral dead-layer. For this adjustment, the FEP efficiencies in the energy range of 302–1770 keV for measurement configuration of the point-like source at a distance of 254 mm were used. These FEP efficiencies were selected because the influence of the top dead-layer and the distance from crystal to front endcap on their values is insignificant. For a change of 2 mm in the thickness of the top dead-layer from the manufacturer's specification, our simulated results showed that the relative deviations in the FEP efficiency are 1.2% at 302.8 keV, 1.1% at 834.8 keV, and 0.98% at 1332.5 keV. Basically, with the photon energy high enough, the attenuation of photon intensity within the absorber layers between the source and the active volume of the detector can be ignored. Therefore, it can be deduced that the effect of the top dead-layer on the FEP efficiencies at high energies is negligible. In addition, the FEP efficiency variations over the whole energy range of 53–1770 keV were always less than 1.52% for changes in the distance from crystal to front endcap up to 2 mm. The FEP efficiency variations due to a change in the distance from crystal to front endcap are mainly related to changes in the solid angle subtended by

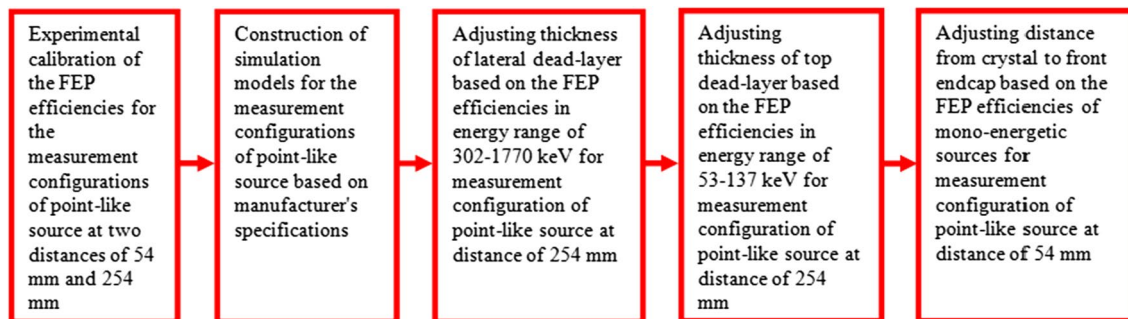


Fig. 2 Overview of the procedure for optimizing the model of p-type HPGe detector

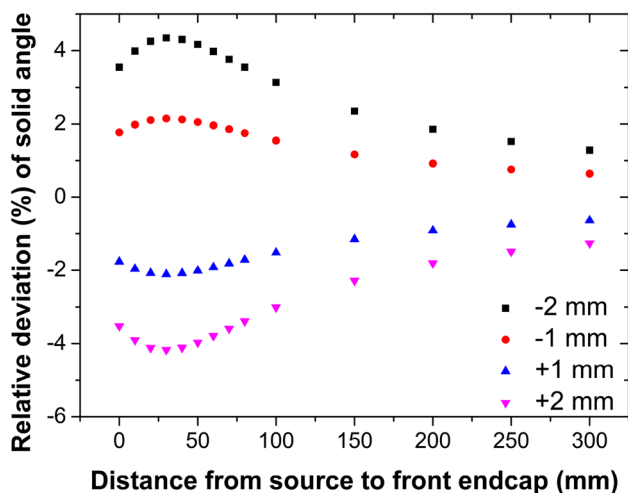


Fig. 3 Relative deviations in the solid angle due to changes of -2 , -1 , $+1$, $+2$ mm in the distance from crystal to front endcap corresponding to the different distances from source to front endcap

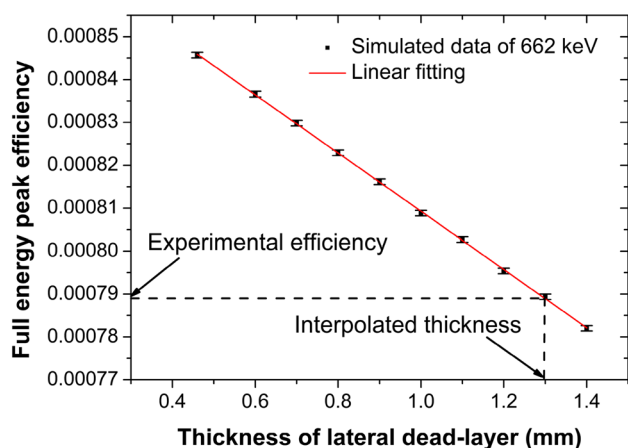


Fig. 4 The linear dependence of the simulated FEP efficiency on the thickness of the lateral dead-layer for the photon energy of 662 keV

the crystal of detector and the source [18]. Figure 3 showed the variations of the relative deviation between solid angle for a given value and solid angle for a nominal value of the distance from crystal to front endcap with the change of the distance from source to front endcap. It can be observed that the relative deviations in the solid angle are insignificant (below 1.5%) at large distances from source to front endcap (above 250 mm). This result implies that the influence of the distance from crystal to front endcap on the FEP efficiency is negligible for the measurement configuration of the point-like source at a considerable distance from source to front endcap.

The second adjustment was made for the thickness of the top dead-layer. For this adjustment, the FEP efficiencies in the energy range of 53–137 keV for measurement

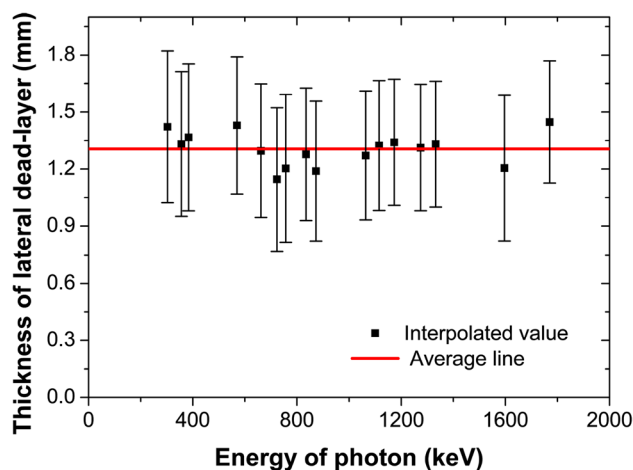


Fig. 5 The interpolated thicknesses of the lateral dead-layer corresponding to the different photon energies in the range of 302–1770 keV

configuration of the point-like source at a distance of 254 mm were used. As mentioned above, these FEP efficiencies can be considered unaffected by the distance from crystal to front endcap. Besides, the FEP efficiencies at low energies are very sensitive to the variations in the thickness of top dead-layer.

The final adjustment was made for the distance from crystal to front endcap. As shown in Fig. 3, the relative deviations in the solid angle are significant at small distances from source to front endcap (below 80 mm). This implies that the FEP efficiencies at such distances are suitable for adjusting the distance from crystal to front endcap. However, it should be taken into consideration that the source placed near the detector will increase the dead-time which affects the quality of the measured spectra. In this study, the FEP efficiencies of mono-energetic sources for measurement configuration of the point-like source at a distance of 54 mm were used for the adjustment of the distance from crystal to front endcap.

Results and discussion

Adjusting the thickness of lateral dead-layer

The FEP efficiencies in the energy range of 302–1770 keV for measurement configuration of the point-like source at a distance of 254 mm were used to adjust the lateral dead-layer. The results calculated for the simulated FEP efficiency with the photon energy of 662 keV were shown in Fig. 4. Clearly, there was a very good linearity between the simulated FEP efficiency and the thickness of the lateral dead-layer. Similar results were also observed for the remaining energies. Therefore, the simulated FEP efficiencies versus the thickness of lateral dead-layer were fitted using the linear

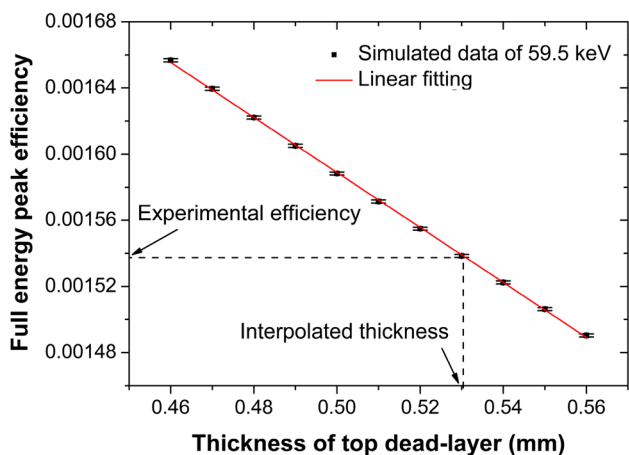


Fig. 6 The linear dependence of the simulated FEP efficiency on the thickness of the top dead-layer for the photon energy of 59.5 keV

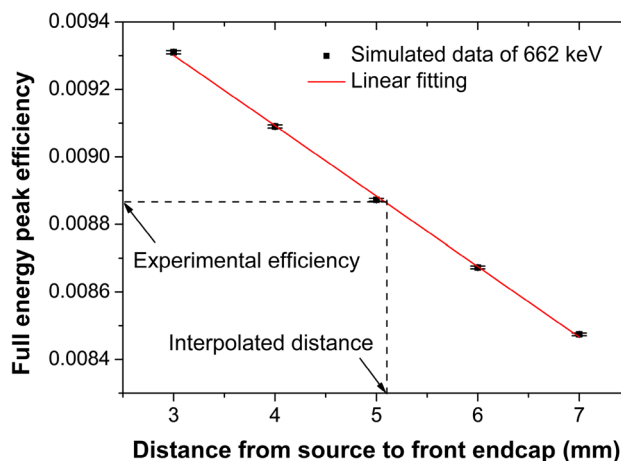


Fig. 8 The linear dependence of the simulated FEP efficiency on the distance from crystal to front endcap for the photon energy of 662 keV

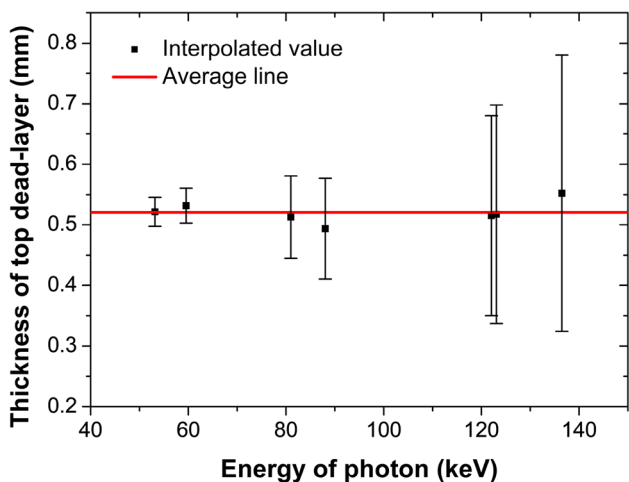


Fig. 7 The interpolated thicknesses of the top dead-layer corresponding to the different photon energies in the range of 53–137 keV

function with the value of the adjusted R-squared of greater than 0.9992 for all investigated photon energies. The thicknesses of the lateral dead-layer were interpolated based on these linear functions and the experimental FEP efficiencies. The interpolated thicknesses corresponding to the different photon energies were shown in Fig. 5. The average of these interpolated thicknesses is 1.31 mm.

Adjusting the thickness of top dead-layer

The FEP efficiencies in the energy range of 53–137 keV for measurement configuration of the point-like source at a distance of 254 mm were used to adjust the top dead-layer. The linear dependence of the simulated FEP efficiency on the thickness of the top dead-layer for the photon energy

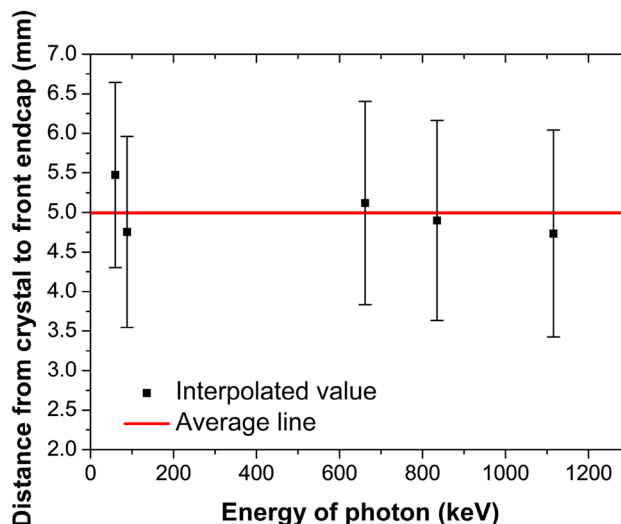


Fig. 9 The interpolated distance from crystal to front endcap corresponding to the different photon energies

of 59.5 keV was shown in Fig. 6. Similar results were also observed for the remaining energies. These data were fitted using the linear function with the value of the adjusted R-squared of greater than 0.9995 for all investigated photon energies. The thicknesses of the top dead-layer were interpolated by substituting the experimental FEP efficiencies into these linear functions. The interpolated thicknesses corresponding to the different photon energies were shown in Fig. 7. It can be observed that the uncertainty of the interpolated thickness increases with increasing photon energy. It is explained that the slope of variation in the FEP efficiency due to change in the thickness of the top dead-layer decreases with higher photon energies. This implies that the use of the FEP efficiencies with low

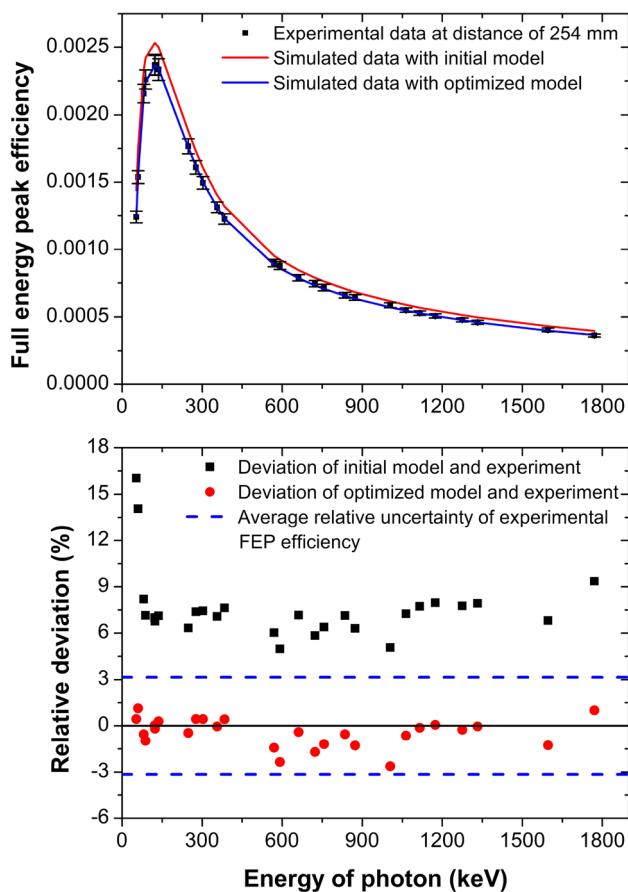


Fig. 10 Comparison between the experimental FEP efficiencies with the simulated FEP efficiencies based on the initial model and the optimized model for measurement configuration of point-like source at distance of 254 mm

photon energies is more suitable for the adjustment of the top dead-layer. The average of these interpolated thicknesses is 0.52 mm. This result showed that the optimized thicknesses of top dead-layer and lateral dead-layer are different.

Adjusting the distance from crystal to front endcap

The FEP efficiencies with photon energies of 60, 88, 662, 835, 1116 keV for measurement configuration of the point-like source at a distance of 54 mm were used to adjust the distance from crystal to front endcap. The results obtained for the simulated FEP efficiency with a photon energy of 662 keV when changing the distance from crystal to front endcap were shown in Fig. 8. The relative variations in the simulated FEP efficiency due to a change in the distance from crystal to front endcap were approximately uniform for photon energies. These data were fitted using the

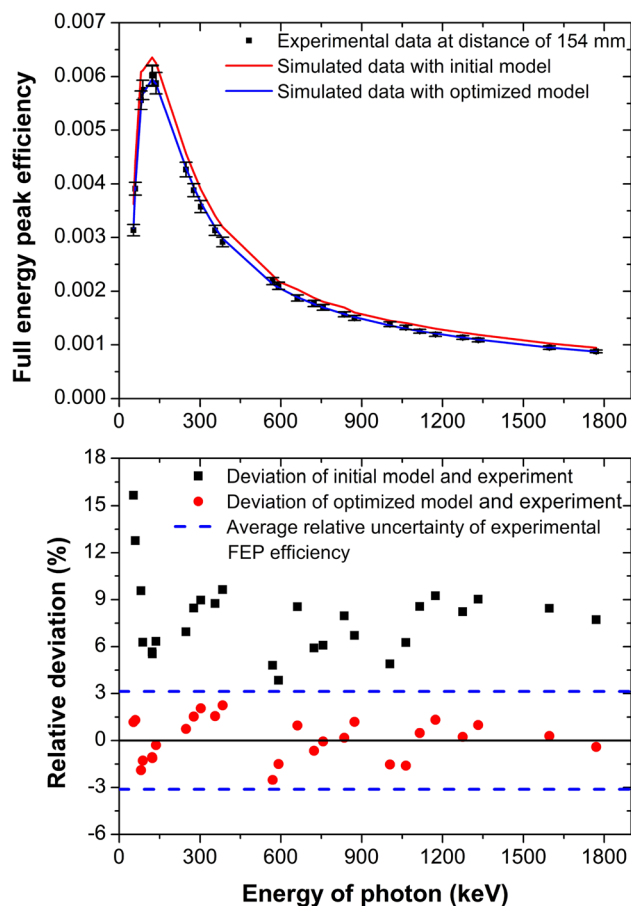


Fig. 11 Comparison between the experimental FEP efficiencies with the simulated FEP efficiencies based on the initial model and the optimized model for measurement configuration of point-like source at distance of 154 mm

linear function with the value of the adjusted R-squared of greater than 0.9991 for all photon energies surveyed. The distances from crystal to front endcap were interpolated by substituting the experimental FEP efficiencies into these linear functions. The interpolated distances corresponding to the different photon energies were shown in Fig. 9. The average of these interpolated distances is 4.99 mm. This optimized value is approximate to the manufacturer's specifications.

Validation of the optimized detector model

The experimental FEP efficiencies in the energy range of 53–1847 keV were compared with the simulated FEP efficiencies based on the initial model and the optimized model in Figs. 10, 11, 12, 13 and 14 for measurement configurations of the point-like source at distances of 54 mm, 154 mm, 254 mm, and S1, S2 cylindrical samples, respectively. The

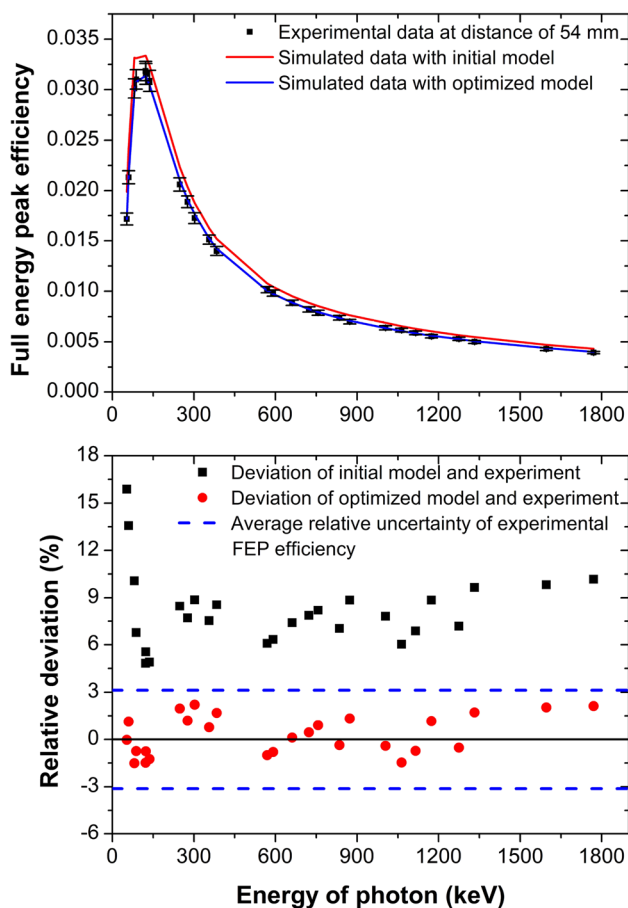


Fig. 12 Comparison between the experimental FEP efficiencies with the simulated FEP efficiencies based on the initial model and the optimized model for measurement configuration of point-like source at distance of 54 mm

upper part of these figures shows the values of the experimental and the simulated FEP efficiencies for different discrete energies (the points are connected by straight lines). Besides, the lower part of these figures shows the relative deviations between the experimental FEP efficiencies and the simulated FEP efficiencies based on the initial model and the optimized model versus the average relative uncertainty of the experimental FEP efficiencies. The dashed line in the lower part represents the average value (%) of the relative uncertainties of the experimental FEP efficiencies for different energies. The relative uncertainties of the experimental FEP efficiencies are about 3.2% for the measurements of the point-like source, 3.1% for the measurement of the S1 sample, and 1.7% for the measurement of the S2 sample.

As can be seen from these figures, there are quite high discrepancies between the experimental FEP efficiencies and the simulated FEP efficiencies based on the initial model. Specifically, the relative deviations are about 6–10% with photon energies above 100 keV and up to 15–19% with a photon energy of 53 keV for all measurement configurations.

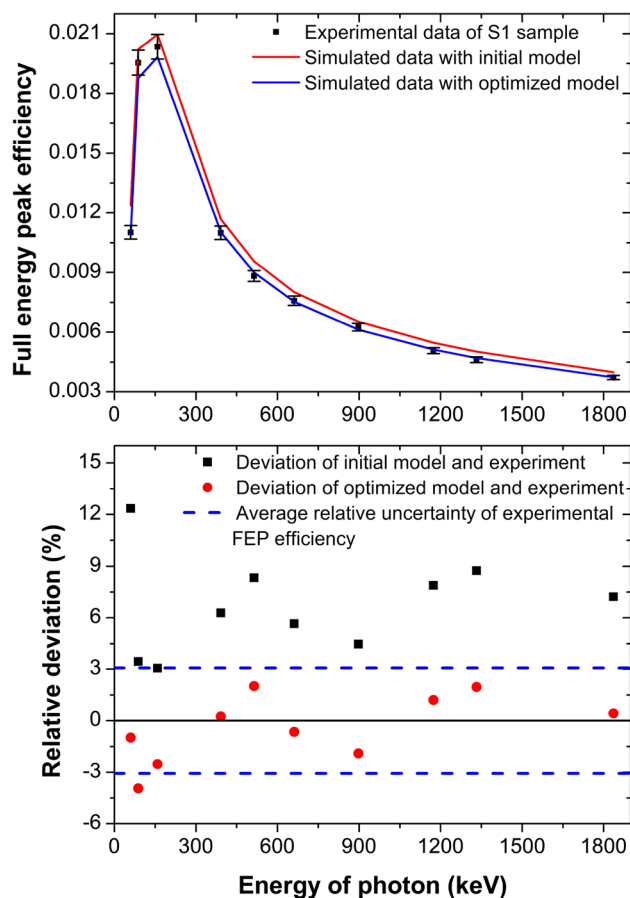


Fig. 13 Comparison between the experimental FEP efficiencies with the simulated FEP efficiencies based on the initial model and the optimized model for measurement configuration of S1 sample

This implies that the accuracy of the initial model is not sufficient for the calculation of FEP efficiency using Monte Carlo simulations.

By using the optimized model, the relative deviations between experimental and simulated FEP efficiencies are less than 4% for all measurement configurations, and the average relative deviation is less than 2%. In most cases, these relative deviations are smaller than the average relative uncertainties of the experimental FEP efficiencies. The comparisons were also done for the photon energy of 46.5 keV from ^{210}Pb in the S1 and S2 samples, but the relative deviations were up to 10%. This may be caused by differences in the element composition and dimensions of the real samples compared to the simulation models. Clearly, the variations in the thickness of the container's wall or the concentration of elements with high atomic number in the sample material can cause a significant change in the FEP efficiency with low photon energy. These results demonstrate that the optimized model is precise and

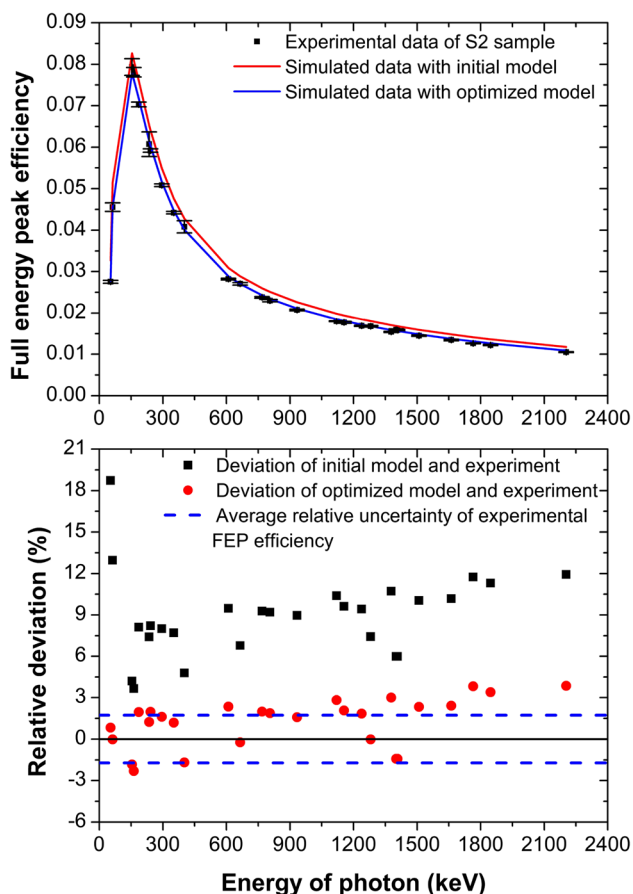


Fig. 14 Comparison between the experimental FEP efficiencies with the simulated FEP efficiencies based on the initial model and the optimized model for measurement configuration of S2 sample

reliable to calculate the FEP efficiency with photon energy in the range of 53–1847 keV using Monte Carlo simulations.

Note that the relative deviation (RD) between the experimental efficiency ($\epsilon_{Exp.}$) and the simulated efficiency ($\epsilon_{Sim.}$) is calculated by the following formula:

$$RD(\%) = \frac{(\epsilon_{Sim.} - \epsilon_{Exp.})}{\epsilon_{Exp.}} \times 100 \quad (3)$$

Conclusions

The present study proposed a procedure for optimizing the model of a coaxial p-type HPGe detector. In this procedure, three parameters of the detector model including the thickness of the lateral dead-layer, the thickness of the top dead-layer and the distance from crystal to front endcap were adjusted based on the interpolation of the experimental FEP efficiencies into the linear functions, which were determined by the fitting of the simulated FEP

efficiencies. The simulated FEP efficiencies obtained by using the optimized detector model showed an excellent agreement with the experimental FEP efficiencies for the measurement configurations of the point-like source and cylindrical sources. The relative deviations between experimental and simulated efficiencies are less than 4% with photon energies in the range of 53–1847 keV. In most of the surveyed cases, these relative deviations are less than the relative uncertainties of the experimental efficiencies. These results verified that the proposed procedure is sufficient to optimize the model of p-type HPGe detector. The advantage of this procedure is that the implementation is quite easy and rapid with simple requirements on experimental conditions. It is recommended that this procedure should be applied for the calibration of the FEP efficiency when the diameter of the analyzed sample is less than the crystal diameter of the detector.

Acknowledgements This research is funded by University of Science, Vietnam National University Ho Chi Minh City under Grant Number T2019-39.

Compliance with ethical standards

Conflict of interest The authors declare that they have no known competing financial interests or personal relationships that could have appeared to influence the work reported in this paper.

References

1. Agostinelli S, Allison J, Amako K et al (2003) GEANT4—a simulation toolkit. *Nucl Instrum Methods Phys Res Sect A* 506:250–303. [https://doi.org/10.1016/S0168-9002\(03\)01368-8](https://doi.org/10.1016/S0168-9002(03)01368-8)
2. Briesmeister JF (2000) MCNP—a general Monte Carlo N-particle transport code. Los Alamos Nat Lab 790
3. Salvat F, Fernández-Vaera JM, Sempau J (2008) PENEL-OPE-2008, A code system for Monte Carlo simulation of electron and photon transport. Nuclear Energy Agency, Spain
4. Thanh TT, Trang HTK, Chuong HD et al (2016) A prototype of radioactive waste drum monitor by non-destructive assays using gamma spectrometry. *Appl Radiat Isot* 109:544–546. <https://doi.org/10.1016/j.apradiso.2015.11.037>
5. Tam HD, Yen NTH, Tran LB, Chuong HD, Thanh TT (2017) Optimization of the Monte Carlo simulation model of NaI(Tl) detector by Geant4 code. *Appl Radiat Isot* 130:75–79. <https://doi.org/10.1016/j.apradiso.2017.09.020>
6. Chuong HD, Thanh TT, Trang LTN et al (2016) Estimating thickness of the inner dead-layer of n-type HPGe detector. *Appl Radiat Isot* 116:174–177. <https://doi.org/10.1016/j.apradiso.2016.08.010>
7. Chuong HD, Hung NQ, Le NTM et al (2019) Validation of gamma scanning method for optimizing NaI(Tl) detector model in Monte Carlo simulation. *Appl Radiat Isot* 149:1–8. <https://doi.org/10.1016/j.apradiso.2019.04.009>
8. Sang TT, Chuong HD, Tam HD (2019) Simple procedure for optimizing model of NaI(Tl) detector using Monte Carlo simulation. *J Radioanal Nucl Chem* 322:1039–1048. <https://doi.org/10.1007/s10967-019-06787-0>

9. Chuong HD, Linh NTT, Trang LTN et al (2020) A simple approach for developing model of Si(Li) detector in Monte Carlo simulation. *Radiat Phys Chem* 166:108459. <https://doi.org/10.1016/j.radphyschem.2019.108459>
10. Bosen J, Agren G, Johansson L (2008) A detailed investigation of HPGe detector response for improved Monte Carlo efficiency calculations. *Nucl Instrum Methods Phys Res Sect A* 587:304–314. <https://doi.org/10.1016/j.nima.2008.01.062>
11. Budjas D, Heisel M, Maneschg W, Simgen H (2009) Optimisation of the MC-model of a p-type Ge-spectrometer for the purpose of efficiency determination. *Appl Radiat Isot* 67:706–710. <https://doi.org/10.1016/j.apradiso.2009.01.015>
12. Agarwal C, Chaudhury S, Goswami A et al (2011) Full energy peak efficiency calibration of HPGe detector for point and extended sources using Monte Carlo code. *J Radioanal Nucl Chem* 287:701–708. <https://doi.org/10.1007/s10967-010-0820-1>
13. Novotny SJ, To D (2015) Characterization of a high-purity germanium (HPGe) detector through Monte Carlo simulation and nonlinear least squares estimation. *J Radioanal Nucl Chem* 304:751–761. <https://doi.org/10.1007/s10967-014-3902-7>
14. Montalván Olivares DM, Guevara MVM, Velasco FG (2017) Determination of the HPGe detector efficiency in measurements of radioactivity in extended environmental samples. *Appl Radiat Isot* 130:34–42. <https://doi.org/10.1016/j.apradiso.2017.09.017>
15. Loan TTH, Ba VN, Thy THN et al (2018) Determination of the dead-layer thickness for both p- and n-type HPGe detectors using the two-line method. *J Radioanal Nucl Chem* 315:95–101. <https://doi.org/10.1007/s10967-017-5637-8>
16. Huy NQ, Binh DQ, An VX (2007) Study on the increase of inactive germanium layer in a high-purity germanium detector after a long time operation applying MCNP code. *Nucl Instrum Methods Phys Res Sect A* 573:384–388. <https://doi.org/10.1016/j.nima.2006.12.048>
17. Gasparro J, Hult M, Johnston PN, Tagziria H (2008) Monte Carlo modelling of germanium crystals that are tilted and have rounded front edges. *Nucl Instrum Methods Phys Res Sect A* 594:196–201. <https://doi.org/10.1016/j.nima.2008.06.022>
18. Vargas MJ, Timon AF, Diaz NC, Sanchez DP (2002) Influence of the geometrical characteristics of an HpGe detector on its efficiency. *J Radioanal Nucl Chem* 253:439–443. <https://doi.org/10.1023/A:1020425704745>
19. Dryak P, Kovar P (2006) Experimental and MC determination of HPGe detector efficiency in the 40–2754 keV energy range for measuring point source geometry with the source-to-detector distance of 25 cm. *Appl Radiat Isot* 64:1346–1349. <https://doi.org/10.1016/j.apradiso.2006.02.083>
20. Cabal FP, Lopez-Pino N, Bernal-Castillo JL et al (2010) Monte Carlo based geometrical model for efficiency calculation of an n-type HPGe detector. *Appl Radiat Isot* 68:2403–2408. <https://doi.org/10.1016/j.apradiso.2010.06.018>
21. Andreotti E, Hult M, Marissens G et al (2014) Determination of dead-layer variation in HPGe detectors. *Appl Radiat Isot* 87:331–335. <https://doi.org/10.1016/j.apradiso.2013.11.046>
22. Haj-Heidari MT, Safari MJ, Afarideh H et al (2016) Method for developing HPGe detector model in Monte Carlo simulation codes. *Radiat Meas* 88:1–6. <https://doi.org/10.1016/j.radmeas.2016.02.035>
23. Hult M, Geelen S, Stals M et al (2019) Determination of homogeneity of the top surface dead layer in an old HPGe detector. *Appl Radiat Isot* 147:182–188. <https://doi.org/10.1016/j.apradiso.2019.02.019>
24. Chham E, García FP, Bardouni TE et al (2015) Monte Carlo analysis of the influence of germanium dead layer thickness on the HPGe gamma detector experimental efficiency measured by use of extended sources. *Appl Radiat Isot* 95:30–35. <https://doi.org/10.1016/j.apradiso.2014.09.007>
25. Jeřkovský M, Javorník A, Breier R et al (2019) Experimental and Monte Carlo determination of HPGe detector efficiency. *J Radioanal Nucl Chem* 322:1863–1869. <https://doi.org/10.1007/s10967-019-06856-4>
26. Tomarchio E, Catania P (2019) Equivalent detector models for the simulation of efficiency response of an HPGe detector with PENELOPE code. *Radiat Eff Defect S* 174:941–953. <https://doi.org/10.1080/10420150.2019.1683833>
27. Goorley T, James M, Booth T et al (2016) Features of MCNP6. *Annals Nucl Ener* 87:772–783. <https://doi.org/10.1016/j.anucene.2015.02.020>
28. LYNX Digital Signal Analyzer, Mirion Technologies Inc. <https://www.mirion.com/products/lynx-digital-signal-analyzer>. Accessed 27 June 2020
29. Detector Lead Shields Model 747 and 747E, Mirion Technologies Inc. <https://www.mirion.com/products/747-747e-lead-shield>. Accessed 27 June 2020
30. Catalogue of reference and calibration sources, Eckert & Ziegler. https://www.ezag.com/fileadmin/user_upload/isotopes/isotopes/Isotrak/isotrak-pdf/Product_literature/EZIPL/EZIP_catalogue_reference_and_calibration_sources.pdf. Accessed 27 June 2020
31. Mixed nuclide solutions, Eckert & Ziegler. https://www.ezag.com/home/products/isotope_products/isotrak_calibration_sources/standardized_solutions/calibrated_solutions/mixed_nuclide_solutions. Accessed 27 June 2020
32. Lépy MC (2004) Presentation of the COLEGRAM software. Note technique LNHB 04/26. Accessed 27 June 2020
33. Recommended data, Laboratoire National Henri Becquerel. http://www.nucleide.org/DDEP_WG/DDEPdata.htm. Accessed 27 June 2020
34. Berlizov A (2009) MCNP-CP: a correlated particle radiation source extension of a general purpose Monte Carlo N-particle transport code. *Appl Model Comput Nucl Sci* 183–194. <https://doi.org/10.1021/bk-2007-0945.ch013>
35. Thanh TT, Vuong LQ, Ho PL et al (2018) Validation of an advanced analytical procedure applied to the measurement of environmental radioactivity. *J Environ Radioact* 184–185:109–113. <https://doi.org/10.1016/j.jenvrad.2017.12.020>
36. Zhu H, Venkataraman R, Menaa N et al (2008) Validation of gamma-ray true coincidence summing effects modeled by the Monte Carlo code MCNP-CP. *J Radioanal Nucl Chem* 278:359–363. <https://doi.org/10.1007/s10967-008-9701-2>

Publisher's Note Springer Nature remains neutral with regard to jurisdictional claims in published maps and institutional affiliations.